On the Effect of Radome Characteristics on Polarimetric Moments and Sun Measurements of a Weather Radar

Jordi Figueras i Ventura, Zaira Schauwecker, Martin Lainer, and Jacopo Grazioli

***Abstract*— This letter illustrates the effects that the regular pattern of the metallic unions of a four-panel radome had on the polarimetric variables [differential reflectivity Z_{dr}, copolar differential phase ϕ_{dp} offset, and copolar correlation coefficient (ρ_{hv})] as well as on the sun measurements of a mobile X-band weather radar. In particular, we focus on the analysis of the spatial distribution of the biases and the temporal variability of the sun measurements. We show that the metallic unions result in a nonnegligible sinusoidal-like spatial variability of the estimated biases (on the order of 7°–8° for ϕ_{dp} offset and 0.4–0.5 dB for Z_{dr} bias), as well as a drop in ρ_{hv} in rain and a large temporal variability in the power measured by sun scans. These effects are compared with the measurements collected without a radome and with the measurements collected with a seamless monoblock radome on the same radar system. It is shown that operating without radome, when possible, has a positive impact on the data quality, largely reducing the spatial variability of the biases and increasing the ρ_{hv} in rain. Similar performances, without the inherent risks, can be obtained as well with a seamless radome. Nevertheless, regardless of the form of operation, we advocate for monitoring the data quality as accurately as possible if quantitative applications are desired.**

***Index Terms*— Data quality, polarimetric weather radar, radome.**

I. Introduction

THE widespread introduction of polarimetric radars has been a game changer for radar meteorology. However, in order to obtain the most from the added information that polarimetry provides, careful monitoring and calibration of the system are required. One important aspect that sometimes may be overlooked is the effects of the radome structure on the quality of the polarimetric variables.

Since 2012, MeteoSwiss operates a mobile X-band Doppler polarimetric weather radar, METEOR 50DX. The system provides, among others, basic polarimetric moments, i.e., reflectivity (horizontal Z_h and vertical Z_v), differential reflectivity (Z_{dr}), copolar correlation coefficient (ρ_{hv}), and raw copolar differential phase (ψ_{dp}) as well as the Doppler moments. It is used for customized applications of specific clients as well as a research and development platform. The system location changes according to the client needs. Since the start of operations, it has been moved to ten different locations within Switzerland on campaigns lasting from few days to over two years. The client applications request the measurements of the upmost accuracy; hence, particular care has been taken to monitor and calibrate the radar.

A few of the issues encountered in the quest for accuracy were related to radome effects. A well-known effect of the radome, particularly at the X-band, is the wet radome attenuation. This is caused by rainfall causing a water coating on the radome that acts as an additional reflective layer and, consequently, reduces the power of the signal that is propagated. This effect has widely been studied in the past. One methodology is to perform empirical measurements with natural or artificial rain. It has been applied to radars working at various frequencies such as C-band [1] or X-band [2], [3]. Others have attempted to model the radome effects, reporting good agreement with actual measurements [4], [5]. Hydrophobic coating of the radome is used to minimize the wet radome effect, but a regular maintenance is required, since the coating ages rapidly. Attempts have been made at correcting radome attenuation by exploiting the self-consistency of the polarimetric variables [6], by correlating the increase in the microwave emissions due to the precipitation at high elevation angles with radome attenuation [7], or by using nearby radars less prone to radome attenuation [8].

Another important effect is caused by the radome structure. Typically, a weather radar radome is formed by several panels lap-joined using metallic threaded unions. If such unions are aligned over a particular orientation (typically vertically oriented), they may have a nonnegligible effect on the quality of the polarimetric variables. Indeed, the metallic unions are reflective and, when aligned, they may reflect more power from one transmitted polarization than the other, consequently disturbing the measurements and causing spatial-dependent biases [9]. To overcome that issue, randomized radome designs have been adopted widely in modern dual-pol radars. However, in order to reduce costs, weather services sometimes opt for keeping the old radomes when adding polarimetric capability to their radar systems. In such a case, attempts at mitigating the problem by using spatial calibration curves have been performed [9]. However, due to the stochastic nature of the radar measurements, there is an inherent uncertainty on the calibration curves, which results in an increase in the overall

Manuscript received September 2, 2019; revised January 9, 2020 and March 13, 2020; accepted March 17, 2020. Date of publication April 29, 2020; date of current version March 25, 2021. *(Corresponding author: Jordi Figueras i Ventura.)*

The authors are with the Swiss Federal Office of Meteorology and Climatology, MeteoSwiss, 6605 Locarno, Switzerland (e-mail: jordi.figuerasiventura@meteoswiss.ch).

This article has supplementary downloadable material available at https://ieeexplore.ieee.org, provided by the authors.

Color versions of one or more of the figures in this letter are available online at https://ieeexplore.ieee.org.

Digital Object Identifier 10.1109/LGRS.2020.2981993

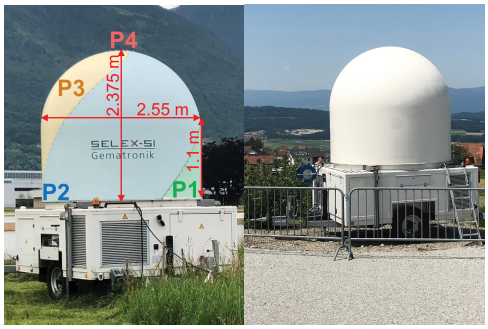

(a) (b)

Fig. 1. (a) Multipanel radome with the four panels (P1–P4) and the dimensions marked. (b) Seamless radome.

measurement uncertainty. Furthermore, it should be mentioned that a similar effect may be due to the near-range objects such as trees, poles, fences, and so on.

The original METEOR 50DX radome has a cylindrical base of 2.55-m diameter and 1.1-m height with a 2.55-m diameter semisphere on the top. The entire radome has a height of 2.375 m. The radome shell has an A-sandwich structure of fiberglass skins with a polyurethane foam core. It is composed of four panels lap-joined by metallic threaded unions. There are three main lateral panels and a small circular panel on the top of the radome. The three unions of the lateral panels start at the base of the radome and reach the top forming a helical shape. As it will be illustrated in this letter, such a configuration was causing the aforementioned spatial calibration bias. A short experiment with the radome off confirmed that the spatial bias was likely due to the metallic union distribution. After discussing with the radar manufacturer, it was decided to install a new seamless radome. The seamless radome features a one-piece structure made of glass fiber-reinforced plastic materials with hydrophobic coating. The radome wall consists of a three-layer sandwich structure. Two shells of molded fiberglass skins cover a foam core to ensure a good stability–weight ratio. The major improvement is in the laminated overlapping panel-joints that are optimized by a structural and electrical tuning. No lightning rods or any lightning-protection cable other than proper grounding of the trailer is used. Fig. 1 shows the original multipanel radome with the four panels color-coded [Fig. 1(a)] and the new seamless one [Fig. 1(b)].

This letter discusses the data-quality-monitoring techniques used at MeteoSwiss in Section II. Section III shows the effects of the multipanel radome on the polarimetric data. Section IV provides a brief discussion on the measurements obtained without any radome. Section V shows the situation with the seamless radome. Section VI provides some conclusions and recommendations.

II. Polarimetric Data-Quality Monitoring at MeteoSwiss

Polarimetric data-quality monitoring at MeteoSwiss is performed by the in-house-developed open-source python-based software Pyrad [10]. Pyrad is a multipurpose radar data-processing framework that can work both in real time and offline. Pyrad can process and visualize data from individual radars as well as composite images. It is capable of ingesting data from all the weather radars in Switzerland, namely, the operational MeteoSwiss C-band network, the MeteoSwiss-operated X-band METEOR 50DX radar, and the EPFL-owned MXPol radar, as well as radar data in the OPERA file format. The signal processing and part of the data visualization are performed by a MeteoSwiss-developed version of the Py-ART radar toolkit that contains enhanced features. MeteoSwiss regularly contributes back to the main Py-ART branch [11] once a new functionality has been thoroughly tested and it is considered of interest for the broad community.

Among the many functionalities implemented by the Pyrad framework, there is an extensive suit of standard data-quality-monitoring techniques. Details on the actual implementation of the techniques discussed in this section can be found in [12]. ρ_{hv} in rain and ϕ_{dp} offset are monitored using similar techniques, as described in [9]. Z_{dr} is monitored using three different techniques: examining the values in precipitation when performing a birdbath scan, checking the value in moderate rain (i.e., 20–22 dBZ) [9], and inspecting its value in aggregates [13]. The absolute reflectivity bias can be estimated using the self-consistency technique described in [14], whereas its evolution in time is monitored by examining the ground clutter in the vicinity of the radar (the so-called relative calibration adjustment) as in [15]. Furthermore, the reflectivity at the colocated gates can be examined in order to ensure the homogeneity of the radar network. All these analyses are typically performed on a daily basis.

Another important reference for monitoring and calibration of radar data is the sun. Precious information can be obtained by examining sun hits such as pointing accuracy [16], antenna beamwidth [17], and gain offset between the horizontally and vertically polarized signal receivers [18]. If sun power is estimated accurately by an independent source [19], also the receiver absolute gain can be retrieved [20]. At MeteoSwiss, two different techniques are used to retrieve data from the sun: The first technique, the so-called sun check, consists of gathering information of all the sun hits occurring during regular radar operations, e.g., nominal antenna pointing angles, receiver noise, radar received sun power, and Z_{dr} as well as sun position and power. A Gaussian fit of the data is then performed over all the sun hits gathered over an arbitrary time period (typically one to three days). The Gaussian fit provides all the information mentioned previously plus the uncertainty of the measurement. The second technique, sun tracking, implies stopping regular operations and pointing the radar antenna toward and area covering the sun in order to obtain the sun pattern. Naturally, this second method is more accurate, but it has the disadvantage that regular operations must be stopped, and therefore, it can only be performed when the radar is not needed for weather surveillance. Uniquely, since the METEOR 50DX is not used for operational weather surveillance, we have been able to implement an automatic sun tracking, which is performed regularly (typically every 30 min), which has proved extremely useful to analyze the radar receiver performance [21].

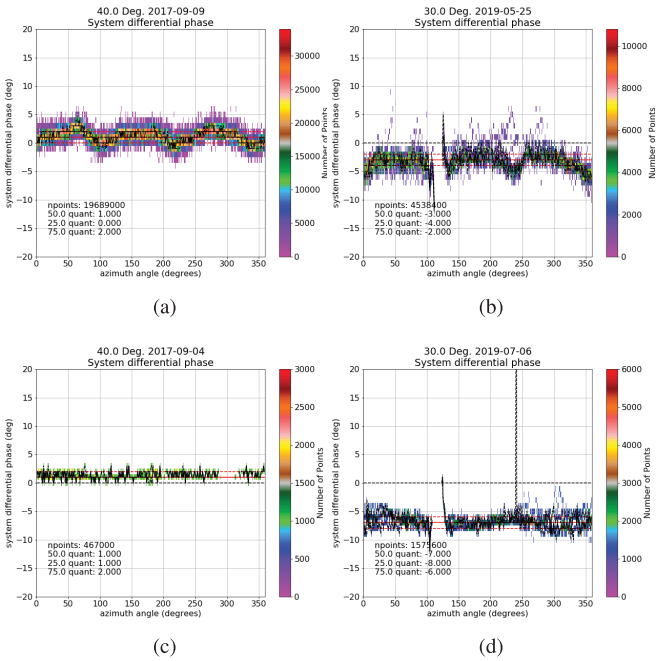

Fig. 2. ϕ_{dp} offset obtained in (a) Meiringen on September 09, 2017 at 40° elevation with the multipanel radome, (b) Torny on May 25, 2019 at 30° elevation with the multipanel radome, (c) Meiringen on September 04, 2017 at 40° without radome, and (d) Torny on July 06, 2019 at 30° elevation with the seamless radome.

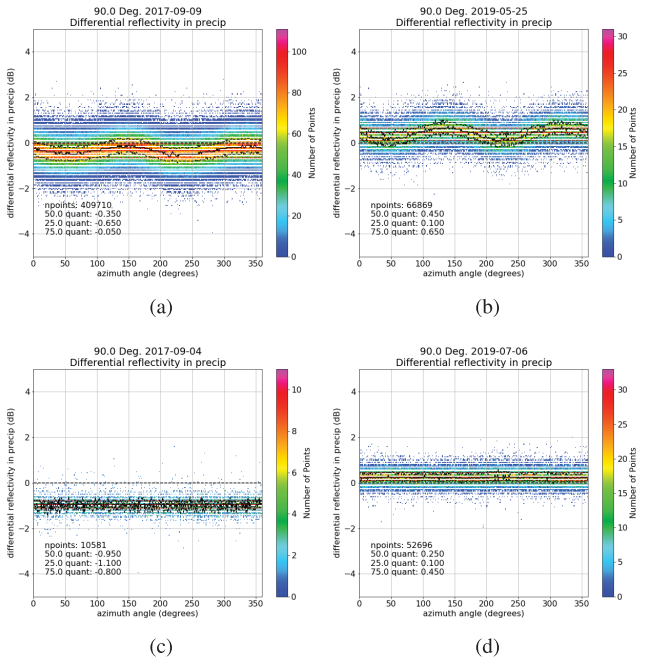

Fig. 3. Similar to Fig. 2 but for Z_{dr} during the birdbath scans obtained in (a) Meiringen on September 09, 2017 with the multi-panel radome, (b) Torny on May 25, 2019 with the multi-panel radome, (c) Meiringen on September 04, 2017 without radome, and (d) Torny on July 06, 2019 with the seamless radome.

III. Effects of the Original Multipanel Radome on the Polarimetric Variables

As mentioned in Section I, throughout the years, the radar has been deployed in ten different sites. In all of them, similar spatial biases have been observed. For illustration purposes, data from two of these sites are shown here: Meiringen (lat 46.743358°, lon 8.109657°, alt 579.8 m a.s.l.) right after the experiment where the radome was removed was completed and Torny (lat 46.769703°, lon 6.953960°, alt 736.0 m a.s.l.). Data from Payerne (lat 46.842473°, lon 6.918370°, alt 454.10 m a.s.l.) are provided as additional material, since it was one of the sites where the radar had better 360° visibility. Likewise, data from Meiringen right before the removal of the radome are also provided as additional material. Meiringen is relevant, since the measuring experiment without any radome described in Section IV was conducted, whereas the radar was placed in Torny when the seamless radome was installed. Figs. 2–4 show the results of the various polarimetric moments' quality monitoring. All the data are presented in a similar manner, i.e., in the form of a density plot of values obtained on a day with precipitation as a function of azimuth for different elevations. The black solid line is the median at each azimuth, while the dashed black lines are the 25th and 75th percentiles, respectively. The red solid line is the median value over all the data obtained at that elevation, and the red dashed lines are the 25th and 75th percentiles.

Fig. 2(a) and (b) clearly shows that the system ϕ_{dp} offset exhibits a sinusoidal azimuthal pattern with three periods. The figures are for elevations 40° and 30°, but similar patterns can be observed at all other elevations. The sinusoidal amplitude may reach 7°–8° and, therefore, is not negligible. The starting point of each period slightly differs at each elevation due to the helical shape formed by the metallic unions. Likewise, it differs from site to site depending on the radar orientation respect to north.

Similar sinusoidal patterns can be observed when measuring the Z_{dr} bias regardless of the measurement technique used. Fig. 3(a) and (b) shows the Z_{dr} biases estimated from the birdbath scans, while Fig. 4(a) and (b) shows the Z_{dr} biases estimated from the measurements in snow at 25° and 23° elevations, respectively. The spatial variability can be as high as 0.4–0.5 dB, well above the 0.2-dB uncertainty recommended for quantitative uses. Estimations in moderate rain (not shown) show similar results. Particularly striking is the azimuthal pattern shown when pointing at the vertical. This has serious implications, since such a measurement is widely used to correct for the system differential gain offset.

Regarding the ρ_{hv} in rain, the value of its 80th percentile for a radar with a good quality antenna should be well above 0.99. With our system, we rarely exceed that value. For example, measurements obtained on September 9, 2017 in Meiringen (not shown) resulted in a value of 0.988 and considerable spatial variation. A low ρ_{hv} results in noisier data.

Radome effects are also observable in the sun-tracking measurements. Fig. 5(a) shows the received sun power in Torny between May 1, 2019 and June 3, 2019, right before the radome was changed. A daily sinusoidal variation is clearly observable on the data. The spread (percentile 16% to percentile 84%) during the period shown is of 0.5 dB. Likewise, a spread of 0.2 dB is observable for the sun Z_{dr} (H channel received sun power minus V channel received sun power, not shown). Scatter plots of the received sun power as a function of sun azimuth and elevation angles with respect to the radar (provided as additional material) show that, although the data are noisy, there is indeed a correlation between the position of the sun with respect to the radar and the received sun power. Again, this has serious implications, since using

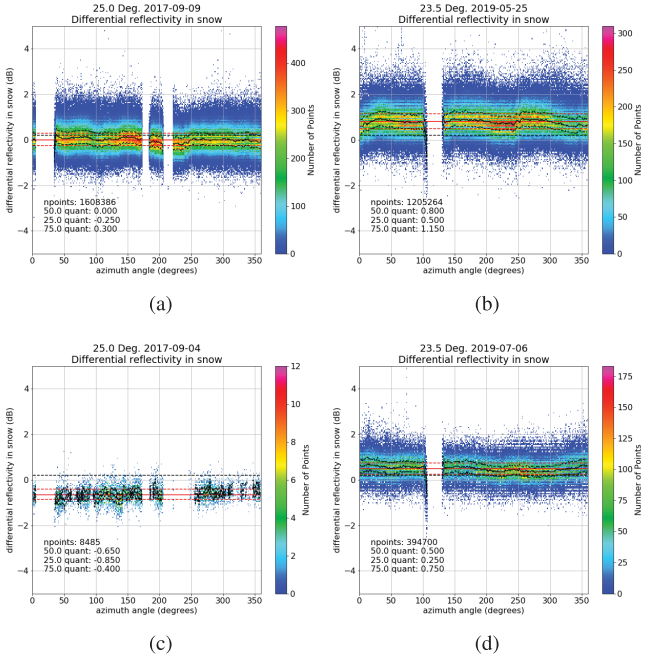

Fig. 4. Similar to Fig. 2 but for Z_{dr} in snow obtained in (a) Meiringen on September 09, 2017 at 25° elevation with the multi-panel radome, (b) Torny on May 25, 2019 at 23.5° elevation with the multi-panel radome, (c) Meiringen on September 04, 2017 at 25° elevation without radome, and (d) Torny on July 06, 2019 at 23.5° elevation with the seamless radome.

the sun as a reference is deemed the most effective way of homogenizing the receiver gain of a radar network.

IV. Data Quality Without Radome

In the course of a measurement campaign in Meiringen, Switzerland, the radome was removed for a short period of time (from September 4 to 7, 2017), allowing to compare the behavior of the polarimetric echoes of precipitation with and without radome. The scanning strategy was exactly the same before, during, and after the radomless experiment. During that short period, there was one day with significant precipitation on September 4, 2017. Data from that day can be seen in Figs. 2(c), 3(c), and 4(c). Although the number of samples is relatively low with respect to other measurements shown in this letter, the benefit of measuring without radome is clear. Indeed, the azimuthal variation is not visible any more in any of the variables considered. Moreover, the ρ_{hv} in the rain 80th percentile increased its value to 0.992. Unfortunately, during the very same period of the radomless experiment, the sun was particularly active, and therefore, no conclusions could be drawn on the impact of operating without radome on the sun measurements.

Those results were convincing enough for MeteoSwiss to seek alternatives for the radome with the manufacturer. One of the proposed solutions was to operate without radome, but we rejected it for mainly two reasons.

1) Without radome, the whole system becomes more vulnerable to wind. Moreover, strong winds may result in a nonuniform antenna-scanning speed and increased vibrations.
2) The radome plays an important part in keeping a stable system temperature. Large variations in temperature may result in significant variations of the receiver gain.

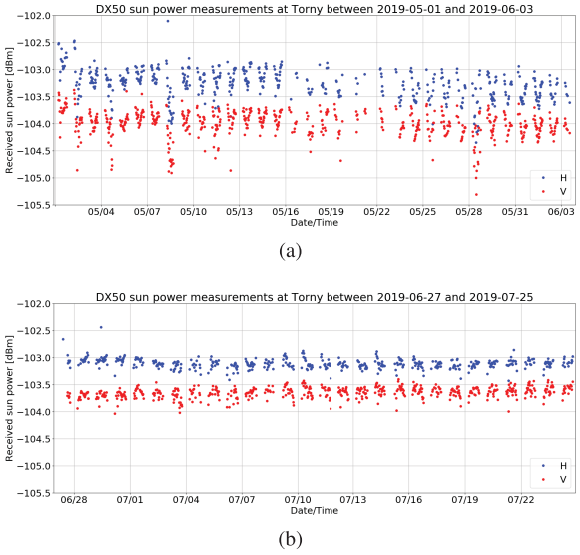

Fig. 5. Sun power measurements obtained in Torny using the sun-tracking technique. (a) Data between May 1, 2019 and June 3, 2019 (multipanel radome). (b) Data between June 27, 2019 and July 25, 2019 (seamless radome).

V. Data Quality With the New Seamless Radome

On April 3, 2019, the radar was moved to Torny and the new seamless radome was installed on June 4, 2019. Shortly thereafter (June 6, 2019), the radar had to be shut down and moved to another location for mandatory trailer revision (the system itself remained untouched). The system was back in operation on the same site (1.7 m apart to be precise) by June 27, 2019. During the whole campaign in Torny, the scanning strategy remained unchanged. As it is illustrated by the example in Figs. 2(d), 3(d), and 4(d), the azimuthal pattern disappeared in all variables. Other examples are provided as additional material. A systematic analysis of all days with sufficient data to get an estimate of the Z_{dr} bias using the birdbath scan in Torny revealed that the median interquantile 25–75 was reduced from 0.65 to 0.45 dB (see additional material). In addition, the ρ_{hv} in the rain 80th percentile increased to the value of 0.992 obtained when operating without radome. Perhaps, the most remarkable difference can be found in the sun power estimated by the sun tracking [see Fig. 5(b)]. The scattering of the values has been reduced dramatically, and no clear diurnal cycle is visible. Indeed, the sun power spread during the period shown was reduced to a mere 0.15 dB, whereas the spread of the sun Z_{dr} was reduced to just 0.1 dB.

One may argue that the improvement is simply due to better hydrophobic coating of the new radome. However, both radomes have the same coating. Moreover, the sinusoidal pattern of the bias with the multipanel radome was observed already back in 2012 when it was purchased (see additional material), so aging effects can be safely excluded. Furthermore, the sun measurements are mostly obtained in dry conditions; therefore, water coating does not play a major effect in the observed results. Uneven surface coating may still result in a spatial variability of the biases in some situations

(strong winds, for example) but what we show here is a dramatic reduction of systematic effects.

VI. Conclusion

This letter illustrated the effects of the radome on the quality of the polarimetric variables of a mobile X-band Doppler polarimetric weather radar. It has been shown that the radome structure has a significant impact on the quality of the polarimetric variables. Such an impact has to be considered when evaluating the quality of the measurements. If the radome panels are placed at preferred orientations and joined by metallic unions, there will be an increase in the spatial variability of the polarimetric variables, typically resulting in sinusoidal-shaped patterns in azimuth. The impact of the radome structure on the Z_{dr} bias and the ϕ_{dp} offset can be partially mitigated by accurately estimating its spatial variation. However, due to the stochastic nature of the radar measurements, the correction curves derived will only be able to account partially for the spatial variability and a higher level of uncertainty will remain. Other impacts of the radome, such as the observed decrease in ρ_{hv}, resulting in an increased noisiness of the data, are much more difficult to correct.

To improve the data quality, one may consider operating the radar without radome. In such a case though, one must be careful to operate it in the conditions of wind speed and temperature that do not disturb the measurements. Such considerations may be simply not possible when 24–7 unattended measurements are desired.

A better approach is to use seamless radomes. One possibility is to use randomly distributed panels, as it is done for most modern dual-pol radars. For smaller radars such as those operating at the X-band, an even better solution may be to use a monoblock radome. In this letter, data-quality-monitoring results of an X-band system operated with a seamless radome have been shown, allowing to conclude that this mode of operation has similar performance as when operating without radome.

It must be mentioned that even though a seamless radome can improve significantly, the radar performance issues remain. One problem is the rain coating of the radome, which may result in significant attenuation. Moreover, strong sustained winds may cause a variable pattern of rain coating resulting in spatially variable attenuation. Regardless of that, nearby objects (e.g., lightning rods) may also influence the quality of the polarimetric variables. For all these reasons, a careful monitoring of the spatial distribution of the polarimetric variables biases is recommended.

Acknowledgment

The authors would like to thank LEONARDO Germany GmbH for their fruitful discussions about alternative radome solutions and the support provided in the installation of the seamless radome.

References

[1] M. Frech, "The effect of a wet radome on dual-pol data quality," in *Proc. 34th AMS Conf. Radar Meteorol.*, Williamsburg, VA, USA, Oct. 2009, p. 13.

[2] R. Bechini, V. Chandrasekar, R. Cremonini, and S. Lim, "Radome attenuation at x-band radar operations," in *Proc. 6th Eur. Conf. Radar Meteorol. Hydrol. (ERAD)*, Sibiu, Romania, Sep. 2010, pp. 1–5.

[3] S. J. Frasier *et al.*, "In-place estimation of wet radome attenuation at x band," *J. Atmos. Ocean. Technol.*, vol. 30, no. 5, pp. 917–928, May 2013, doi: 10.1175/JTECH-D-12-00148.1.

[4] J. L. Salazar-Cerreño *et al.*, "A drop size distribution (DSD)-based model for evaluating the performance of wet radomes for dual-polarized radars," *J. Atmos. Ocean. Technol.*, vol. 31, no. 11, pp. 2409–2430, Nov. 2014, doi: 10.1175/JTECH-D-13-00208.1.

[5] J. Díaz, J. L. Salazar-Cerreno, A. Mancini, and J. G. Colom, "Multilayer radome design and experimental characterization of scattering and propagation properties for atmospheric radar applications," in *Proc. 5th Conf. Transition Res. Oper.*, Phoenix, AZ, USA, 2015, pp. 1–5. [Online]. Available: https://ams.confex.com/ams/95Annual/webprogram/Manuscript/Paper259871/AMS%20PAPER.pdf

[6] E. Gorgucci, R. Bechini, L. Baldini, R. Cremonini, and V. Chandrasekar, "The influence of antenna radome on weather radar calibration and its real-time assessment," *J. Atmos. Ocean. Technol.*, vol. 30, no. 4, pp. 676–689, Apr. 2013, doi: 10.1175/JTECH-D-12-00071.1.

[7] R. Thompson and A. Illingworth, "Correcting attenuation in operational radars from both heavy rain and the radome using the observed microwave emission," in *Proc. 7th Eur. Conf. Radar Meteorol. Hydrol. (ERAD)*, Toulouse, France, 2012, p. 1.

[8] J. M. Trabal, I. Zawadski, and D. J. McLaughling, "A method to correct for wet radome attenuation in casa radars by the use of a contiguous wsr-88d radar," in *Proc. 5th Eur. Conf. Radar Meteorol. Hydrol.*, Helsinki, Finland, Jun. 2008.

[9] J. Figueras i Ventura, A.-A. Boumahmoud, B. Fradon, P. Dupuy, and P. Tabary, "Long-term monitoring of French polarimetric radar data quality and evaluation of several polarimetric quantitative precipitation estimators in ideal conditions for operational implementation at C-band," *Quart. J. Roy. Meteorolog. Soc.*, vol. 138, no. 669, pp. 2212–2228, Oct. 2012.

[10] J. Figueras i Ventura, A. Leuenberger, Z. Kuensch, J. Grazioli, and U. Germann, "Pyrad: A real-time weather radar data processing framework based on Py-art," in *Proc. 38th AMS Conf. Radar Meteorol.*, Chicago, IL, USA, Aug. 2017, p. 1.

[11] J. J. Helmus and S. M. Collis, "The Python ARM radar toolkit (Py-ART), a library for working with weather radar data in the Python programming language," *J. Open Res. Softw.*, vol. 4, Jul. 2016.

[12] J. Figueras i Ventura, "Data quality monitoring with Pyrad," Federal Office Meteorol. Climatol. MeteoSwiss, Locarno, Switzerland, Tech. Rep., 2018. [Online]. Available: https://github.com/meteoswiss-mdr/pyrad/blob/master/doc/pyrad_monitoring_fvj.pdf

[13] M. J. Dixon, J. C. Hubbert, and S. Ellis, "A zdr calibration check using hydrometeors in the ice phase," in *Proc. 38th AMS Conf. Radar Meteorol.*, Chicago, IL, USA, 2017, pp. 1–15.

[14] J. J. Gourley, A. J. Illingworth, and P. Tabary, "Absolute calibration of radar reflectivity using redundancy of the polarization observations and implied constraints on drop shapes," *J. Atmos. Ocean. Technol.*, vol. 26, no. 4, pp. 689–703, Apr. 2009.

[15] V. Louf *et al.*, "An integrated approach to weather radar calibration and monitoring using ground clutter and satellite comparisons," *J. Atmos. Ocean. Technol.*, vol. 36, no. 1, pp. 17–39, Jan. 2019, doi: 10.1175/JTECH-D-18-0007.1.

[16] A. Huuskonen and I. Holleman, "Determining weather radar antenna pointing using signals detected from the sun at low antenna elevations," *J. Atmos. Ocean. Technol.*, vol. 24, no. 3, pp. 476–483, Mar. 2007, doi: 10.1175/JTECH1978.1.

[17] A. Huuskonen, M. Kurri, H. Hohti, H. Beekhuis, H. Leijnse, and I. Holleman, "Radar performance monitoring using the angular width of the solar image," *J. Atmos. Ocean. Technol.*, vol. 31, no. 8, pp. 1704–1712, Aug. 2014, doi: 10.1175/JTECH-D-13-00246.1.

[18] I. Holleman, A. Huuskonen, R. Gill, and P. Tabary, "Operational monitoring of radar differential reflectivity using the sun," *J. Atmos. Ocean. Technol.*, vol. 27, no. 5, pp. 881–887, May 2010, doi: 10.1175/2010JTECHA1381.1.

[19] K. F. Tapping, "The 10.7 cm solar radio flux (F10.7)," *Space Weather*, vol. 11, no. 7, pp. 394–406, Jul. 2013, doi: 10.1002/swe.20064.

[20] I. Holleman, A. Huuskonen, M. Kurri, and H. Beekhuis, "Operational monitoring of weather radar receiving chain using the sun," *J. Atmos. Ocean. Technol.*, vol. 27, no. 1, pp. 159–166, Jan. 2010, doi: 10.1175/2009JTECHA1213.1.

[21] M. Gabella and A. Leuenberger, "Dual-polarization observations of slowly varying solar emissions from a mobile X-Band radar," *Sensors*, vol. 17, no. 5, p. 1185, 2017. [Online]. Available: https://www.mdpi.com/1424-8220/17/5/1185